Dalton
www.rsc.org/dalton

Electronic influence of ligand substituents on the rate of polymerization of ε-caprolactone by single-site aluminium alkoxide catalysts †

Luis M. Alcazar-Roman, Brendan J. O'Keefe, Marc A. Hillmyer * and William B. Tolman *
Department of Chemistry, University of Minnesota, 207 Pleasant St. SE, Minneapolis, MN 55455-0431, USA. E-mail: hillmyer@chem.umn.edu; tolman@chem.umn.edu

Received 4th April 2003, Accepted 10th June 2003
First published as an Advance Article on the web 1st July 2003

A series of novel five-coordinate aluminium mono alkoxide complexes supported by ^{R1,R2}BPBA (bis-3-R^1-5-R^2-phenoxymethyl-bisamine) ligands were synthesized to probe the effect of electronic variation in the supporting ligand on the rate of ε-caprolactone polymerization. Substitution on the aromatic position *para* to the phenoxide donor oxygen by *tert*-butyl, methoxy and bromo substituents furnished aluminium complexes that catalyzed the polymerization of ε-caprolactone at different rates. We propose that a subtle interplay between complex Lewis acidity and alkoxide nucleophilicity determines the overall rate of polymerization in these systems.

Introduction

Metal alkoxide complexes have been used with great success for the ring opening polymerization of cyclic ester monomers, including those derived from biorenewable resources (*e.g.*, lactide).[1] So-called single-site catalysts based on aluminium,[2–8] magnesium,[9,10] iron,[11,12] and zinc[13–16] exhibit good polymerization rates and can lead to excellent molecular weight and stereochemical control. While there is a wealth of information about the mechanisms of cyclic ester polymerizations by simple homoleptic metal alkoxides (such as Al(O-*i*-Pr)$_3$),[11,17–30] mechanistic information for catalysis by metal alkoxide complexes modified by the presence of ancillary ligands is less abundant.[11,14–16,31] While in principle the polymerization activity of a catalyst can be influenced by the steric and electronic characteristics of the ancillary ligand framework, the effect of electronic perturbations of the supporting ligand (particularly in systems that exhibit parity with respect to steric effects) on the rate of propagation is not well established. Gibson and coworkers have shown that modification of the supporting ligand by introduction of electron-withdrawing substituents furnishes a more active aluminium catalyst for the polymerization of lactide.[6] They argue that the decreased electron-donating ability of the ligand increases the electrophilicity of the metal center, thus enhancing the activity of the catalyst. On the other hand, Spassky and coworkers observed similarly enhanced reactivity for a catalyst with a related ligand, but lacking the electron-withdrawing ligand substituent.[2] In a different system used for the copolymerization of CO_2 and epoxides, Coates and coworkers observed that electron withdrawing substituents on the supporting ligand greatly improved the catalytic efficiency of the Zn complex used.[32]

To further examine these phenomena and establish the relationship between electronic effects and polymerization activity, we have synthesized a series of aluminium complexes supported by the bis(phenolato)bis(amine) (^{R1,R2}BPBA)[33,34] ligand framework and an isopropoxide initiator (Fig. 1). The ^{R1,R2}BPBA^{2-} ligand set, a member of which had been used previously for Zr-catalyzed olefin polymerizations,[33,34] was chosen because it was anticipated to lead to mononuclear single-initiator catalysts. Moreover, the H$_2$^{R1,R2}BPBA precursor is easily prepared in one step from simple reagents, thus allowing for the systematic variation of the electronic and steric properties of the phenolic portion and access to a varied set of aluminium complexes. Here we present a systematic study of ligand electronics on the propagation rate using discrete, single-site aluminium catalysts for the polymerization of ε-caprolactone (ε-CL, Scheme 1).

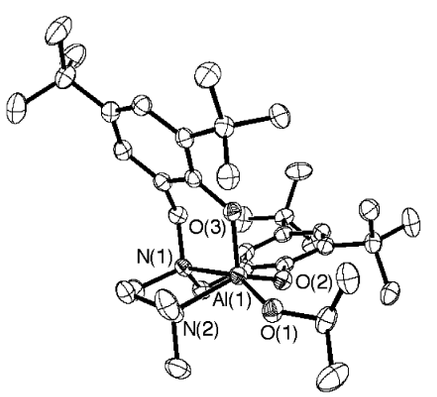

Fig. 1 X-Ray structure of **3a**, with all non-hydrogen atoms shown as 50% thermal ellipsoids (hydrogen atoms omitted for clarity).

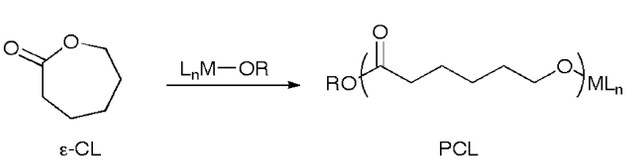

Scheme 1

Results and discussion

Synthesis of ligands and complexes

Ligands H$_2$$^{t\text{-Bu},t\text{-Bu}}$BPBA (**2a**), H$_2$$^{t\text{-Bu,OMe}}$BPBA (**2b**) and H$_2$$^{t\text{-Bu,Br}}$BPBA (**2c**) were synthesized using a modified Mannich condensation protocol outlined in Scheme 2.[33] A *tert*-butyl group was chosen as the R^1 substituent in order to favor mononuclear complex formation and limit chain aggregation during polymerization reactions. Substituent R^2 was varied to obtain ligands containing phenolate moieties with differing electron donating abilities. Isolation of the crude solids followed by recrystallization afforded analytically pure samples of **2a**–**c** in moderate to good yields. This method did not furnish satisfactory yields of

† Electronic supplementary information (ESI) available: Fig. S1: X-Ray structure of **3b**; Fig. S2: X-Ray structure of **3c**; Fig. S3: ^{1}H NMR lineshape analysis for **3a**; Fig. S4: Eyring plot for temperature-dependent fluxional process for **3a**. Table S1: Selected bond lengths and angles for **3b**; Table S2: Selected bond lengths and angles for **3c**. See http://www.rsc.org/suppdata/dt/b3/b303760f/

DOI: 10.1039/b303760f

Table 1 Selected bond lengths (Å) and angles (°) for ($^{t\text{-Bu},t\text{-Bu}}$BPBA)-Al(O-*i*-Pr) (**3a**)

Al(1)–O(1)	1.7359(10)	Al(1)–O(2)	1.7842(10)
Al(1)–O(3)	1.7589(10)	Al(1)–N(1)	2.1969(12)
Al(1)–N(2)	2.1177(13)		
O(1)–Al(1)–O(2)	97.15(5)	O(1)–Al(1)–O(3)	108.89(5)
O(2)–Al(1)–O(3)	109.71(5)	O(1)–Al(1)–N(2)	83.59(5)
O(3)–Al(1)–N(2)	103.23(5)	O(2)–Al(1)–N(2)	144.70(5)
O(1)–Al(1)–N(1)	154.19(5)	O(3)–Al(1)–N(1)	93.04(4)
O(2)–Al(1)–N(1)	87.68(4)	N(2)–Al(1)–N(1)	78.12(4)

Estimated standard deviations are in parentheses.

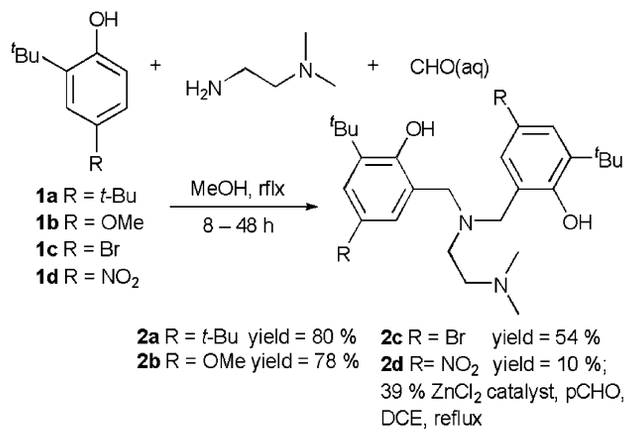

Scheme 2 Synthesis of ligands **2a**–**d**

ligand $H_2{}^{t\text{-Bu},NO_2}$BPBA (**2d**), presumably due to the electron deficiency of the aromatic ring of phenol **1d**. Even when conducting the reaction in refluxing *n*-butanol solvent for upwards of 96 h **2d** was isolated in only *ca.* 10% yield. However, a more reasonable yield of **2d** (39%, unoptimized) was achieved by using an aprotic reaction medium, paraformaldehyde as the methylene source, and $ZnCl_2$ as a catalyst (see Experimental).

Complexes ($^{t\text{-Bu},t\text{-Bu}}$BPBA)Al(O-*i*-Pr) (**3a**), ($^{t\text{-Bu},OMe}$BPBA)-Al(O-*i*-Pr) (**3b**) and ($^{t\text{-Bu},Br}$BPBA)Al(O-*i*-Pr) (**3c**) were synthesized by heating a toluene solution of ligand and aluminium isopropoxide for at least 12 h (Scheme 3). Complexes **3a**–**c** were isolated as crystalline solids in good yield (45–75%). X-Ray crystal structures of **3a**–**c** revealed similar topologies for the three complexes, with all four donors of the ^{R1,R2}BPBA ligand bound to a single Al center (**3a** is shown in Fig. 1, **3b** and **3c** in ESI, † Figs. S1 and S2). Metrical parameters are summarized in Tables 1 (**3a**), S1 (**3b**), and S2 (**3c**). The coordination geometry in **3a** is distorted square pyramidal with a τ-value[35] of 0.16. One of the phenolate arms of the supporting ligand occupies the apical position, while the isopropoxide and the remaining $^{t\text{-Bu},t\text{-Bu}}$BPBA ligand donors occupy the equatorial sites. Slightly different geometries are adopted in **3b** and **3c**, which are best described as distorted halfway between square pyramidal and trigonal bipyramidal (τ-values for **3b** and **3c** = 0.61). Viewed in the former sense, the dimethylamino donor arm of the $^{t\text{-Bu},OMe}$BPBA and $^{t\text{-Bu},Br}$BPBA

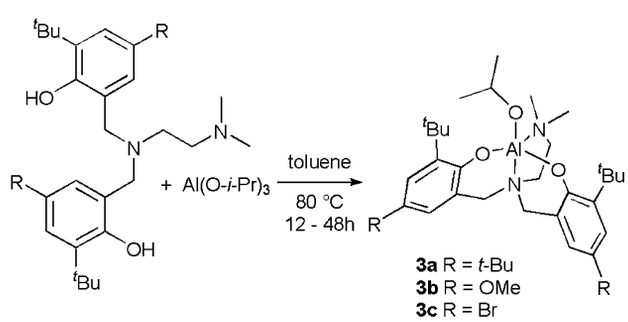

Scheme 3 Synthesis of aluminium complexes **3a**–**c**

Table 2 Comparison of selected bond lengths (Å) for ($^{t\text{-Bu},t\text{-Bu}}$BPBA)-Al(O-*i*-Pr) (**3a**), ($^{t\text{-Bu},OMe}$BPBA)Al(O-*i*-Pr) (**3b**) and ($^{t\text{-Bu},Br}$BPBA)Al-(O-*i*-Pr)·1/2(C_7H_8) (**3c**)

	3a	**3b**	**3c**
Al(1)–O(1)	1.7359(10)	1.7441(11)	1.7408(19)
Al(1)–O(2)	1.7842(10)	1.7597(11)	1.7642(19)
Al(1)–O(3)	1.7589(10)	1.7694(11)	1.7806(19)
Al(1)–N(1)	2.1969(12)	2.1083(13)	2.153(2)
Al(1)–N(2)	2.1177(13)	2.1818(13)	2.099(2)

Estimated standard deviations are in parentheses.

ligands occupies the apical position, while the isopropoxide ligand and the remainder of the donors of the supporting ligands occupy equatorial positions. Importantly in the context of the present examination of ligand electronic effects on polymerization activity, consideration of the Al–(O-*i*-Pr) bond lengths or the Al–O and Al–N bond distances corresponding to the phenolate or amine donors of the supporting ligands for the three complexes (Table 2) reveals no discernable relationship with the electron donating characteristics of the different phenolate groups.

Complex **3d** could not be directly prepared by reaction of Al(O-*i*-Pr)$_3$ with **2d**. Under the same reaction conditions used to prepare **3a**–**c**, only deprotonated **2d** was isolated. In an alternative approach, reaction of a THF suspension of **2d** with $AlMe_3$ (2.0 M solution in heptane) produced a dark orange solution with simultaneous release of a gas, presumably methane. However, addition of 1.1 equiv. of isopropanol to this solution only produced deprotonated **2d**. Thus, while metathesis reactions to generate the deprotonated ligand **2d** and isopropanol or methane appear to occur readily, the deprotonated $^{t\text{-Bu},NO_2}$BPBA^{2-} ligand appears to lack the necessary electron donating ability to stabilize the [Al(O-*i*-Pr)]$^{2+}$ fragment.

The ^{1}H NMR spectrum for **3a** in CD_2Cl_2 recorded at 25 °C is less complicated than expected given its solid-state structure, suggesting that it is stereochemically non-rigid.[36] Upon cooling the sample to −85 °C, broadening and then resharpening of the resonances corresponding to the $^{t\text{-Bu},t\text{-Bu}}$BPBA ligand was observed, with a decoalescence temperature, T_c = −45 °C. At −85 °C the ^{1}H NMR spectrum is consistent with a static square pyramidal structure corresponding to the X-ray structure obtained for the compound. ^{1}H NMR spectra obtained between −85 an −35 °C were analyzed with WINDNMR Pro,[37] using two singlet resonances (low temperature limit) corresponding to a *tert*-butyl group that collapse into a single resonance at ambient temperature. Rate constants for the exchange process were obtained by spectral simulation using the built-in pairwise-exchange matrix (ESI, † Fig. S3). An Eyring plot yielded activation barriers $\Delta H^{\ddagger}$ = 6.9 ± 0.6 kJ mol^{-1} and $\Delta S^{\ddagger}$ = −21 ± 3 J mol^{-1} K^{-1} ($\Delta G^{\ddagger}$ = 7.0 ± 0.9 kJ mol^{-1}, 298 K), values typical of an intramolecular process. The data are consistent with fast interconversion between two degenerate square-pyramidal geometries that allow for the exchange of the phenoxide arms of the ligand from axial to equatorial positions, and thus chemical site exchange of the α-methylene and aromatic protons associated with the phenoxide groups. This exchange may be envisaged to occur through a trigonal bipyramidal transition state, following a ligand-restricted pseudorotation or turnstile mechanism.

Polymerization of ε-caprolactone by 3a–c

Complexes **3a**–**c** are effective for the controlled polymerization of ε-caprolactone (ε-CL; Scheme 1).[38] Samples of polycaprolactone (PCL) were prepared by dissolving ε-CL ([ε-CL]$_0$ ≈ 1.0 M) and initiator in toluene at room temperature. Plots of the number average molecular weight (M_n) *vs.* ([ε-CL]$_0$ − [ε-CL]$_t$)/[Al]$_0$ (Fig. 2) as well as plots of M_n *vs.* % ε-CL conversion (Fig. 3) are linear (similar data were obtained for **3b** and

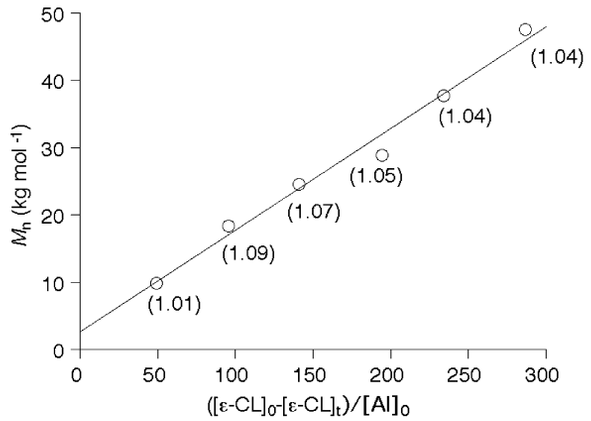

Fig. 2 Number average molecular weight (SEC) of PCL as a function of monomer consumed to catalyst ratio for the polymerization of ε-CL by **3a**. Polydispersities (PDI) are indicated in parentheses. Conditions: $[\varepsilon\text{-CL}]_0 = 1.0$ M for all data, [**3a**] = 20.0, 10.0, 6.7, 5.0, 4.0 and 3.3 mM, 25 °C, toluene, all conversions >95%.

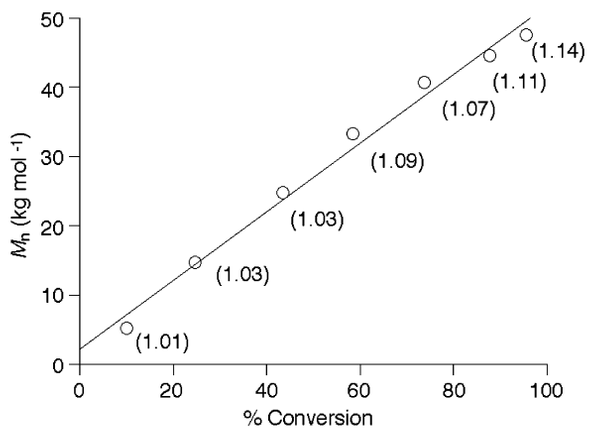

Fig. 3 Number average molecular weight as a function of conversion of ε-CL. Polydispersities (PDI) are indicated in parentheses. Conditions: $[\varepsilon\text{-CL}]_0 = 1.0$ M, $[\mathbf{3a}]_0 = 10.0 \times 10^{-3}$ M, 25 °C, toluene.

3c, not shown). The polydispersity indices (PDI) of polymer samples obtained using **3a**, **3b** or **3c** as the catalysts are narrow (1.03–1.11); SEC chromatograms of the product polymers exhibit narrow unimodal peaks. End-group analysis (^{1}H NMR spectroscopy) of a PCL sample prepared with an initial monomer to catalyst (**3a**) ratio of 50 : 1 showed that all isopropoxide moieties initiate polymerization efficiently. A polymerization reinitiation experiment with **3a** showed that the aluminium-capped chains of PCL were capable of enchaining additional monomer units. The resulting polymer showed no evidence of the original PCL sample and the increase in the polydispersity index was modest (initial PDI: 1.04, final: 1.10), as shown in Fig. 4. To summarize, the polymerization of ε-CL by **3a** shows many of the characteristics of a living polymerization with fast and efficient initiation.

Kinetic analysis of the polymerization of ε-Cl by 3a–c

Conversion of ε-CL to PCL was monitored by *in situ* IR spectroscopy (ReactIR). Plots of absorbance *vs.* time for both decay of ε-CL and growth of PCL followed a single exponential decay for five half-lives, indicating a first-order dependence on monomer concentration and no appreciable catalyst decomposition during the course of the polymerization reaction (Fig. 5). Rate constants obtained by varying the initial concentration of catalyst/initiator show that the polymerization reaction is first order in catalyst (Fig. 6). A lower catalyst concentration threshold was found in all three cases, under which polymerization does not occur (approx. 1.0×10^{-3} M).[11,16] This lower concentration threshold varied little with different

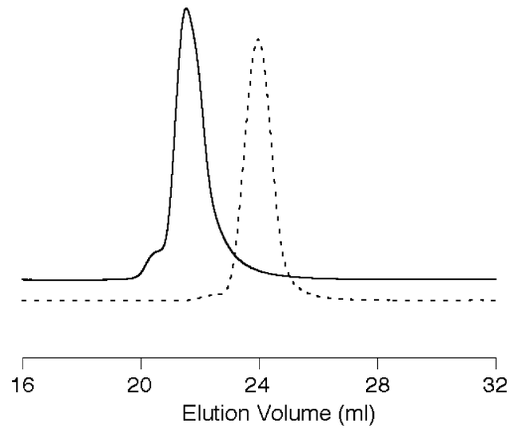

Fig. 4 SEC data for polymerization reinitiation experiment. (---) Trace for PCL (99.7% conversion) for $[\varepsilon\text{-CL}]_0 = 1.0$ M, $[\mathbf{3a}]_0 = 10.0$ mM, 25 °C, $M_n = 21.8 \times 10^3$ g mol^{-1}, PDI = 1.04. (—) Trace for PCL after subsequent addition of 200 equiv. ε-CL, 96.4% conversion, $M_n = 51.9 \times 10^3$ g mol^{-1}, PDI = 1.10.

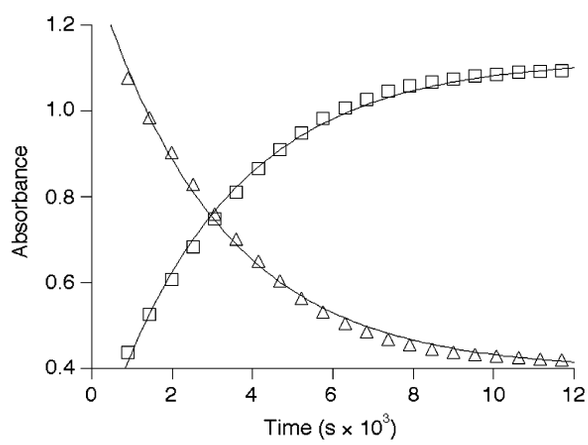

Fig. 5 Typical kinetic plot for the polymerization of ε-CL by **3a**, with data (every other point shown) for ε-CL shown as triangles and for PCL shown as squares. Conditions: $[\varepsilon\text{-CL}]_0 = 1.0$ M, **3a** = 20.0×10^{-3} M, 25 °C, toluene.

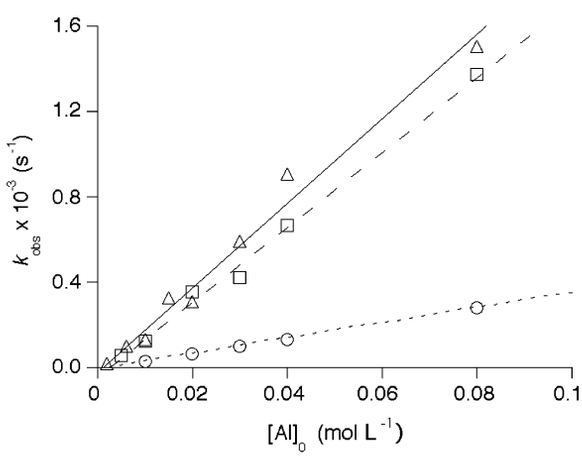

Fig. 6 Determination of the order in catalyst for the polymerization of ε-Cl by **3a** (triangles), **3b** (squares), and **3c** (circles). Each data point is the average of at least three different experiments. Conditions: $[\varepsilon\text{-CL}]_0 = 1.0$ M, 25 °C, toluene.

batches of solvent and monomer. Once the catalyst concentration is corrected to account for the concentration of this presumably deactivating impurity, double logarithmic plots of k_{obs} *vs.* catalyst concentration were linear and displayed slopes with values very close to unity. These results confirm a first order dependence on catalyst concentration and provide strong evidence against kinetically significant aggregation of the aluminium-capped PCL chains when **3a**–**c** are used as catalysts.

Table 3 Propagation rate constants (k_p) for the polymerization of ε-CL

Catalyst	$10^{-3}k_p/s^{-1}$ mol^{-1} L
3a	19.80(4)
3b	17.50(4)
3c	3.57(3)

Conditions: $[\varepsilon\text{-CL}]_0$ = 1.0 M, 25.0 °C, toluene. Standard deviations are noted in parentheses.

The propagation rate constants (k_p) were obtained from the slopes of the k_{obs} *vs.* $[Al]_0$ plots (Table 3). In general, the k_p values are approximately an order of magnitude smaller than reported for Al(O-*i*-Pr)$_3$ and Et$_2$AlOEt (0.62 and 0.14 M^{-1} s^{-1}, respectively),[39,40] but are similar to that cited for Fe(OCHPh$_2$)(amidinate)$_2$ (0.05 M^{-1} s^{-1}).[11] Surprisingly, the bromo-substituted complex **3c** displays the slowest rate of propagation amongst the set **3a**–**c**; k_p for polymerization catalyzed by **3c** is 5.5 times smaller than that for reactions where **3a** is used. In addition, k_p for the *tert*-butyl (**3a**) and methoxy (**3b**) substituted catalysts are similar, the value for the latter being only slightly smaller than for the former.

We were surprised to find that the electron-withdrawing bromide substituents on the ancillary ligand, expected to increase the Lewis acidity of the metal center, actually reduce the rate of enchainment of the monomer. Although we have not independently assessed the Lewis acidity of **3a**–**c**, it seems that for catalysts that polymerize cyclic esters, Lewis acidity is not the largest or only factor in determining the overall activity of the catalyst. The propagation rate constant (k_p) is a composite of several fundamental steps. The fundamental rate constants for monomer binding (and dissociation), nucleophilic attack by the coordinated alkoxide onto the coordinated ester carbonyl, and the rearrangements that result in the final ring opening of monomer all contribute to the value of k_p. It is possible that with an increase in Lewis acidity, and the concomitant increase of the equilibrium constant for monomer binding, other changes occur that reduce the rate of subsequent steps in the mechanism, such as attack of the coordinated alkoxide ligand on the ester carbonyl of the monomer. One such perturbation would be an increase in the strength of the bond between the metal center and the propagating alkoxide ligand. Such a change would render the alkoxide ligand progressively less nucleophilic as the Lewis acidity of the metal is increased. Conversely, the greater nucleophilicity of the alkoxide in the less Lewis acidic **3b** (R = OMe) might be offset by the diminished ability to bind monomer. This could explain the comparable activity of **3a** (R = *tert*-butyl) and **3b**. In fact, there is presumably an optimum Lewis acidity that gives the best combination of monomer binding and alkoxide nucleophilicity in this system, thus leading to the highest overall rate of polymerization. Other changes that could affect k_p are increases in the barriers of reorganization for the conformational changes the catalyst must undergo as the monomer binds and is subsequently attacked by the alkoxide group and rearranges to form the ring opened product. Tighter binding of the ancillary ligand induced by decreased electron density at the metal would increase the activation energy required to reorganize the metal–ligand bonds that comprise the coordination sphere of the metal center.

Conclusion

Through a comparative study of the polymerization behavior of a series of structurally well-defined aluminium catalysts supported by ligands with essentially identical steric profiles but differing electron donating abilities, we have been able to discern an unexpected electronic effect on polymerization activity. Both decreasing and increasing the electron density around the metal (relative to **3a**, R = *tert*-butyl) actually *decreased* the propagation rate constant (k_p) for the ring opening polymerization of ε-CL, with the effect of R = Br being the most significant. We infer that changes of the electron-donating ability of the supporting ligand have a more complicated effect on the mechanism of the polymerization reaction than previously assumed, and that, by extension, decreasing the electron density at a catalytic metal site may not necessarily result in an increase in ring opening polymerization efficiency for other cyclic esters either.

Experimental

General considerations

All reactions were carried out under an inert atmosphere using standard Schlenk and drybox techniques, unless otherwise indicated. All reagents were obtained from commercial suppliers and used as received unless otherwise indicated. ε-CL was purified by distillation from CaH_2 and stored under N_2. Deuteriated solvents were dried over CaH_2, distilled under vacuum and stored under N_2. Protiated solvents were dried and degassed by passing through columns containing activated alumina under positive argon pressure. ^{1}H NMR spectra were recorded on a Varian VXR-300 or VI-300 and referenced to residual protiated solvent. Variable-temperature ^{1}H NMR spectra were recorded on the Varian VXR-300 instrument. Sample temperature was calibrated using the standard methanol NMR thermometer.[41,42] ^{13}C{^{1}H} NMR spectra were recorded on a Varian VI-300 or a Varian VI-500 and are referenced to residual protium in the solvent. Line-shape analysis was performed with WINDNMR Pro.[37] IR spectra were obtained with an ASI ReactIR 4000, equipped with a DiComp 6-bouce ATR probe. Size exclusion chromatography (SEC) data were recorded on a HP 1100 high pressure liquid chromatography (HPLC) with a flow rate of 1.00 mL s^{-1} at 40 °C using THF as the eluent. The columns were calibrated against polystyrene standards. The HPLC was equipped with a HP refractive index detector and three Jordi polydivinylbenzene columns of 10^4, 10^3 and 100 Å pore sizes. Elemental analyses were determined by Atlantic Microlab, Inc., Norcross, GA, and Robertson Microlit Laboratories, Inc., Madison, NJ. Ligand **2a**,[33] 4-bromo-2-*tert*-butylphenol,[43] and 4-nitro-2-*tert*-butylphenol,[44] were prepared by published methods.

Ligand synthesis

***N*,*N*-Bis[methyl(2-hydroxy-3-*tert*-butyl-5-methoxyphenyl)]-*N′*,*N′*-dimethylethylenediamine 2b.** A procedure identical to that used to prepare **2a** was followed, except using 2-*tert*-butyl-4-methoxyphenol (9.05 g, 50.2 mmol), *N*,*N*-dimethylethylenediamine (2.22 g, 25.2 mmol), and formaldehyde solution (5.66 mL, 69.6 mmol). The product was recrystallized from CH_2Cl_2–methanol at 0 °C (9.32 g, 78.3% yield). ^{1}H NMR (300 MHz, $CDCl_3$): δ 1.37 (s, 18H), 2.27 (s, 6H), 2.56 (br, 1H), 3.57 (s, 4H), 3.74 (s, 6H), 6.47 (d, 2H, J = 3.0 Hz), 6.79 (d, 2H, J = 3.0 Hz), 9.42 (br, 2H) ppm. ^{13}C{^{1}H} NMR (75.48 MHz, $CDCl_3$): δ 29.54, 35.19, 44.14, 44.86, 55.76, 55.83, 56.33, 112.68, 113.35, 123.16, 138.63, 149.82, 151.60 ppm. Anal. Calc. for $C_{28}H_{44}N_2O_4$: C, 71.15; H, 9.38; N, 5.93. Found: C, 70.80; H, 9.43; N, 5.91%.

***N*,*N*-Bis[methyl-(2-hydroxy-3-*tert*-butyl-5-bromophenyl)]-*N′*,*N′*-dimethylethylenediamine 2c.** A procedure identical to that used to prepare **2a** was followed, except using 2-*tert*-butyl-4-bromophenol (10.0 g, 43.7 mmol), *N*,*N*-dimethylethylenediamine (1.92 g, 21.8 mmol), and formaldehyde (4.92 mL, 60.7 mmol), with a 72 h reflux. The product was recrystallized from CH_2Cl_2–methanol at 0 °C (6.89 g, 54.0% yield). ^{1}H NMR (300 MHz, CD_2Cl_2): δ 1.34 (s, 18H), 2.27 (s, 6H), 2.57 (s, 4H), 3.54 (s, 4H), 7.05 (d, 2H, J = 2.5 Hz), 7.27 (d, 2H, J = 2.5 Hz), 10.32 (br,

Table 4 X-Ray data collection and processing parameters[a]

	3a	3b	3c
Empirical formula	$C_{37}H_{61}AlN_2O_3$	$C_{31}H_{49}AlN_2O_5$	$C_{29}H_{43}AlBr_2N_2O_3 \cdot 0.5C_7H_8$
M_r	608.86	556.70	700.52
Crystal system	Orthorhombic	Triclinic	Triclinic
Space group	*Pbcn*	$P\bar{1}$	$P\bar{1}$
Z	8	2	2
a/Å	19.4598(15)	10.3444(11)	10.1742(11)
b/Å	15.2420(12)	12.6782(13)	13.0089(14)
c/Å	24.583(2)	12.9992(13)	14.1058(15)
α/°	90	79.554(2)	111.851(2)
β/°	90	77.283(2)	94.902(2)
γ/°	90	66.203(2)	99.557(2)
V/Å^3	7291.5(10)	1513.4(3)	1686.5(3)
D_c/Mg m^{-3}	1.109	1.222	1.379
μ/mm^{-1}	0.091	0.108	2.463
Reflections collected	58561	15122	16745
Independent reflections (R_{int})	6449 (0.0336)	5374 (0.0303)	5965 (0.0287)
Observed reflections	5460	4472	4725
Data/restraints/parameters	6449/0/404	5374/0/364	5965/52/377
Goodness-of-fit on F^2	1.030	1.058	1.025
Final R indices[b]	$R1 = 0.0350$, $wR2 = 0.0875$	$R1 = 0.0355$, $wR2 = 0.0899$	$R1 = 0.0342$, $wR2 = 0.0831$
Largest diff. peak, hole/e Å^{-3}	0.220, −0.253	0.226, −0.241	0.689, −0.487

[a] All structures determined at 173K, Mo-Kα radiation, refinement based on F^2. [b] For $I > 2\sigma(I)$, $R1 = \Sigma||F_o| - |F_c||/\Sigma|F_o|$, and $wR2 = [\Sigma[w(F_o^2 - F_c^2)^2]/\Sigma[w(F_o^2)^2]]^{1/2}$, where $w = 1/\sigma^2(F_o^2) + (aP)^2 + bP$.

2H) ppm. $^{13}C\{^1H\}$ NMR (75.48 MHz, CD_2Cl_2): δ 29.49, 35.47, 44.90, 49.43, 55.80, 55.91, 110.70, 125.34, 130.00, 131.06, 140.17, 155.61 ppm. Anal. Calc. for $C_{26}H_{38}Br_2N_2O_2$: C, 54.75; H, 6.71; N, 4.91. Found: C, 54.80, H, 6.76; N, 4.95%.

***N*,*N*-Bis[methyl-(2-hydroxy-3-*tert*-butyl-5-nitrophenyl)]-*N*′,*N*′-dimethylethylenediamine 2d.** 2-*tert*-Butyl-4-nitrophenol (15.0 g, 76.8 mmol), *N*,*N*-dimethylethylenediamine (3.39 g, 38.4 mmol), paraformaldehyde (3.21 g, 100 mmol), and zinc chloride (524 mg, 3.84 mmol) were dissolved in approx. 30 mL of dichloroethane and placed under a nitrogen atmosphere. This mixture was then heated to a gentle reflux for 12 h. The mixture was then allowed to cool to room temperature, and methanol (10 mL) was added. An orange precipitate formed. The mixture was stirred at room temperature for a further 20 min and the product was collected by filtration and recrystallized from CH_2Cl_2 at 0 °C (7.54 g, 39.0% yield). ^1H NMR (300 MHz, CD_2Cl_2): δ 1.43 (s, 18H), 2.52 (s, 6H), 2.90 (s, 4H), 3.41 (s, 4H), 8.25 (d, 2H, $J = 1.8$ Hz), 8.88 (d, 2H, $J = 1.8$ Hz), 12.02 (br, 2H) ppm. $^{13}C\{^1H\}$ NMR (75.48 MHz, CD_2Cl_2): δ 25.66, 35.40, 45.16, 49.72, 56.21, 56.43, 118.45, 122.00, 136.73, 137.95, 161.10, 163.34 ppm. Anal. Calc. for $C_{26}H_{38}N_4O_6$: C, 62.13; H, 7.62; N, 11.15. Found: C, 61.87, H, 7.39; N, 10.83%.

(*t*-Bu,*t*-BuBPBA)Al(O-*i*-Pr) (3a). Aluminium isopropoxide (400 mg, 1.96 mmol) and **2a** (1.03 g, 1.96 mmol) were weighed into a 15 mL pressure tube and suspended in approximately 3 mL of toluene. A stir bar was added, the vessel was capped with a screw-threaded PTFE cap fitted with an o-ring, and the mixture was heated at 85 °C for 48 h. Solvent was removed under reduced pressure and the residue was redissolved in a minimum volume of toluene, layered with pentane and allowed to stand at −34 °C. the product was obtained as a white solid (878 mg, 73.6% yield). Crystals suitable for X-ray structure determination were obtained from slow evaporation of concentrated toluene solution at room temperature. ^1H NMR (300 MHz, CD_2Cl_2): δ 1.19 (d, 6H, $J = 3.0$ Hz), 1.21 (s, 18H), 1.42 (s, 18H), 2.66 (app. s, 8H), 2.80 (app. t, 2H), 3.47 (app. d, 2H), 3.63 (br, 2H), 4.65 (sept., 1H, $J = 5.9$ Hz), 6.80 (d, 2H, $J = 2.6$ Hz), 7.20 (d, 2H, $J = 2.6$ Hz) ppm. $^{13}C\{^1H\}$ NMR (125.7 MHz, CD_2Cl_2): δ 28.64, 30.03, 32.07, 34.46, 35.51, 49.63, 50.70, 55.99, 59.62, 62.66, 121.97, 124.17, 124.20, 138.19, 139.00, 156.30 ppm. Anal. Calc. for $C_{37}H_{61}AlN_2O_3$: C, 72.99; H, 10.10; N, 4.60. Found: C, 72.60; H, 9.89; N, 4.59%.

(*t*-Bu,OMeBPBA)Al(O-*i*-Pr) (3b). Aluminium isopropoxide (216 mg, 1.06 mmol) and **2b** (500 mg, 1.06 mmol) were weighed into a 15 mL pressure tube, the mixture suspended in approximately 3 mL of toluene and heated at 85 °C for 48 h as in the preparation of **3a**. X-Ray quality crystals of **3b** formed from the reaction medium upon slow cooling to room temperature. After crystal selection, the bulk mixture was cooled further to −34 °C and decanted. The crystals were then suspended in approx. 2 mL of toluene, and reheated in the sealed reaction vessel until the solution became homogeneous. An off-white white crystalline solid was obtained upon cooling to −34 °C. (403 mg, 68.0% yield). ^1H NMR (300 MHz, CD_2Cl_2): δ 1.18 (d, 6H, $J = 6.0$ Hz), 1.41 (s, 18H), 2.65 (m, 8H), 2.79 (app. t, 2H), 3.44 (app. d, 2H), 3.62 (m, 2H), 3.68 (s, 6H), 4.64 (sept, 1H, $J = 5.9$ Hz), 6.39 (d, 2H, $J = 3.1$ Hz), 6.78 (d, 2H, $J = 3.2$ Hz) ppm. $^{13}C\{^1H\}$ NMR (125.7 MHz, CD_2Cl_2): δ 28.61, 29.84, 35.48, 49.56, 50.59, 56.05, 56.22, 59.38, 62.66, 112.05, 114.07, 122.71, 140.24, 150.82, 152.82 ppm. Anal. Calc. for $C_{31}H_{49}AlN_2O_5$: C, 66.88; H, 8.87; N, 5.03. Found: C, 66.52; H, 8.73; N, 4.82%.

(*t*-Bu,BrBPBA)Al(O-*i*-Pr) (3c). Aluminium isopropoxide (1.31 g, 6.42 mmol) and **3c** (3.75 g, 6.42 mmol) were weighed into a 15 mL pressure tube and suspended in approximately 3 mL of toluene. Heating and workup proceeded as for the preparation of **3b**, except the crystals of the product obtained were suspended in pentane and stirred to remove the solvent of crystallization to yield a fine white powder that was collected by filtration. (1.87 g, 44.6% yield). ^1H NMR (300 MHz, CD_2Cl_2) δ 1.18 (d, 6H, $J = 5.9$ Hz), 1.18 (s, 18H), 2.65 (m, 8H), 2.79 (app. t, 2H), 3.42 (m, 2H), 3.61 (m, 2H), 4.62 (sept, 1H, $J = 5.9$ Hz), 6.96 (d, 2H, $J = 2.5$ Hz), 7.27 (d, 2H, $J = 2.6$) ppm. $^{13}C\{^1H\}$ NMR (125.7 MHz, CD_2Cl_2) δ 28.50, 29.65, 35.51, 49.59, 50.68, 55.90, 58.65, 62.75, 108.60, 124.77, 129.88, 130.34, 141.97, 158.01 ppm. Anal. Calc. for $C_{29}H_{43}AlBr_2N_2O_3$: C, 53.22; H, 6.62; N, 4.28. Found: C, 53.51; H, 6.90; N, 4.03%.

Polymerization of ε-CL. ε-CL (143 mg, 1.26 mmol), and the appropriate amount of catalyst to obtain the desired monomer to initiator ration were weighed into a silylated glass screw-cap vial. Toluene solvent was then added to obtain an approximate concentration of ε-CL of 1 M. A stir bar was added and the vial was capped using a PTFE-lined septum cap. The reaction was allowed to stir at room temperature. Conversion was

determining by observing the ^{1}H NMR resonances of polymer and monomer by withdrawing small aliquots of the homogeneous reaction mixture and dissolving them in $CDCl_3$ in air. Reactions were precipitated with pentane and precipitated polymer was washed with cold pentane and dried under vacuum.

Kinetic measurements. A silylated vessel with a 24/40 inner ground glass joint was loaded with ε-caprolactone (288 mg, 2.51 mmol) followed by an appropriate volume of toluene. A stir bar was added, and the solution was stirred thoroughly to ensure proper mixing. Then, a solution of catalyst was added via syringe, the vessel was fitted onto the probe of an ASI ReactIR 4000 instrument and brought out of the glove box. Data acquisition was started immediately after assembly of the apparatus, resulting in dead-times on the order of 1–1.5 min. IR data was acquired and analyzed in absorbance mode. The program ConcIRT was used to perform a global fit of the collected spectra to known spectra of ε-caprolactone, poly-caprolactone, and solvent. Plots of absorbance *vs.* time obtained in this manner furnished observed rate constants that were identical to those obtained from plots of the absorbance value at a fixed frequency relative to that of an unchanging baseline point. Pseudo-first-order rate constants were calculated by fitting global absorbance values to the equation $A = A_0e^{-kt} + c$, where k is the observed rate constant k_{obs} and t is the time in seconds.

X-Ray crystallography. Single crystals of ($^{t\text{-}Bu,t\text{-}Bu}$BPBA)Al(O-*i*-Pr) (**3a**), ($^{t\text{-}Bu,OMe}$BPBA)Al(O-*i*-Pr) (**3b**, and ($^{t\text{-}Bu,Br}$BPBA)Al(O-*i*-Pr)·0.5C_7H_8 (**3c**) were selected from the bulk material, mounted in inert oil and transferred to the cold gas stream of the diffractometer. Table 4 provides a summary of the crystallographic data. Data were collected on Siemens and Bruker SMART Platform difractometers using ω-scans. The intensity data were corrected for absorption and decay (SADABS).[45] Final cell constants were calculated from the *xyz* centroids of strong reflections from the actual data collection after integration (SAINT).[46] The structures were solved by direct methods and they were refined based on *F2* using SHELXS-97 and SHELXL-97.[47]

CCDC reference numbers 207604–207606.

See http://www.rsc.org/suppdata/dt/b3/b303760f/ for crystallographic data in CIF or other electronic format.

Acknowledgements

We thank the NSF (CHE 9975357) and the David and Lucille Packard Foundation for financial support.

References

1 B. J. O'Keefe, M. A. Hillmyer and W. B. Tolman, *J. Chem. Soc., Dalton Trans.*, 2001, 2215.
2 A. Bhaw-Luximon, D. Jhurry and N. Spassky, *Polym. Bull.*, 2000, **44**, 31.
3 T. M. Ovitt and G. W. Coates, *J. Polym. Sci. A, Polym. Chem.*, 2000, **38**, 4686.
4 T. M. Ovitt and G. W. Coates, *J. Am. Chem. Soc.*, 1999, **121**, 4072.
5 C. P. Radano, G. L. Baker and M. R. Smith, *J. Am. Chem. Soc.*, 2000, **122**, 1552.
6 P. A. Cameron, D. Jhurry, V. C. Gibson, A. J. P. White, D. J. Williams and S. Williams, *Macromol. Rapid Commun.*, 1999, **20**, 616.
7 D. Chakraborty and E. Y.-X. Chen, *Organometallics*, 2002, **21**, 1438.
8 H. Chen, B. Ko, B. Huang and C. Lin, *Organometallics*, 2001, **20**, 5076.
9 M. H. Chisholm, N. W. Eilerts, J. C. Huffman, S. S. Iyer, M. Pacold and K. Phomphrai, *J. Am. Chem. Soc.*, 2000, **122**, 11845.
10 M. H. Chisholm, J. C. Huffman and K. Phomphrai, *J. Chem. Soc., Dalton Trans.*, 2001, 222.
11 B. J. O'Keefe, L. E. Breyfogle, M. A. Hillmyer and W. B. Tolman, *J. Am. Chem. Soc.*, 2002, **124**, 4384.
12 V. C. Gibson, E. L. Marshall, D. Navarro-Llobet, A. J. P. White and D. J. Williams, *J. Chem. Soc., Dalton Trans.*, 2002, 4321.
13 M. Cheng, A. B. Attygalle, E. B. Lobkovsky and G. W. Coates, *J. Am. Chem. Soc.*, 1999, **121**, 11583.
14 B. M. Chamberlain, M. Cheng, D. R. Moore, T. M. Ovitt, E. B. Lobkovsky and G. W. Coates, *J. Am. Chem. Soc.*, 2001, **123**, 3229.
15 L. R. Rieth, D. R. Moore, E. B. Lobkovsky and G. W. Coates, *J. Am. Chem. Soc.*, 2002, **124**, 15239.
16 C. K. Williams, N. R. Brooks, M. A. Hillmyer and W. B. Tolman, *Chem. Commun.*, 2002, 2132.
17 A. Duda, *Macromolecules*, 1996, **29**, 1399.
18 A. Kowalski, A. Duda and S. Penczek, *Macromolecules*, 1998, **31**, 2114.
19 H. R. Kricheldorf, *Chemosphere*, 2001, **43**, 46.
20 G. Montaudo, M. S. Montaudo, C. Puglisi, F. Smaperi, N. Spassky, A. LeBorgne and M. Wisniewski, *Macromolecules*, 1996, **29**, 6461.
21 A. Kowalski, A. Duda and S. Penczek, *Macromolecules*, 2000, **33**, 689.
22 A. Kowalski, J. Libiszowski, A. Duda and S. Penczek, *Macromolecules*, 2000, **33**, 1964.
23 A. Kowalski, A. Duda and S. Penczek, *Macromolecules*, 2000, **33**, 7359.
24 S. Penczek, T. Biela and A. Duda, *Macromol. Rapid Commun.*, 2000, **21**, 941.
25 P. Dubois, N. Ropson, R. Jérôme and P. Teyssié, *Macromolecules*, 1996, **29**, 1965.
26 J. L. Eguiburu, M. J. Fernandez-Berridi, F. P. Cossío and J. San Román, *Macromolecules*, 1999, **32**, 8252.
27 W. M. Stevels, M. J. K. Ankoné, P. J. Dijkstra and J. Feijen, *Macromolecules*, 1996, **29**, 6132.
28 Y. Wang and M. A. Hillmyer, *Macromolecules*, 2000, **33**, 7395.
29 R. F. Storey and J. W. Sherman, *Macromolecules*, 2002, **35**, 1504.
30 B. J. O'Keefe, S. M. Monnier, M. A. Hillmyer and W. B. Tolman, *J. Am. Chem. Soc.*, 2001, **123**, 339.
31 K. B. Aubrecht, M. A. Hillmyer and W. B. Tolman, *Macromolecules*, 2002, **35**, 644.
32 D. R. Moore, M. Cheng, E. B. Lobkovsky and G. W. Coates, *Angew. Chem., Int. Ed.*, 2002, **41**, 2599.
33 T. Toupance, S. R. Duberley, N. H. Rees, B. R. Tyrrell and P. Mountford, *Organometallics*, 2002, **21**, 1367.
34 E. Y. Tshuva, I. Goldberg, M. Kol and Z. Goldschmidt, *Organometallics*, 2001, **20**, 3017.
35 A. W. Addison, T. R. Rao, J. Reedijk, J. van Rijn and G. C. Verschoor, *J. Chem. Soc., Dalton Trans.*, 1984, 1349.
36 Pulsed Gradient Spin Echo (PGSE) measurements of the diffusion coefficient of **3a** indicate that it is a monomer in CD_2Cl_2 solution at concentrations similar to those used in the polymerization reactions described herein (C. K. Williams, L. E. Breyfogle, S.-K. Choi, W.-W. Nam, M. A. Hillmyer and W. B. Tolman, *J. Am. Chem. Soc.*, submitted). Monomer–dimer equilibria thus do not appear to underly the observed VT-NMR behavior.
37 WINDNMR Pro: NMR Spectrum Calculations V7.1.5, H. J. Reich, Madison, Wisconsin, 2000.
38 Complexes **3a**–**c** did not polymerize D,L-lactide at ambient temperature or at 80 °C in CH_2Cl_2 or toluene solution, respectively, nor was any appreciable conversion to polymer observed under melt conditions (140 °C).
39 A. Duda and S. Penczek, *Macromolecules*, 1995, **28**, 5981.
40 S. Penczek, A. Duda and T. Biela, *Polym. Prepr. (Am. Chem. Soc., Div. Polym. Chem.)*, 1994, **35**(2), 508.
41 A. L. Van Geet, *Anal. Chem.*, 1968, **42**, 679.
42 D. S. Raiford, C. L. Fisk and E. D. Becker, *Anal. Chem.*, 1979, **51**, 2050.
43 J. Berthelot, C. Guette, P. L. Desbene, J. J. Basselier, P. Chaquin and D. Masure, *Can. J. Chem.*, 1989, **67**, 2061.
44 G. G. I. Moore and A. R. Kirk, *J. Org. Chem.*, 1979, **44**, 925.
45 R. Blessing, *Acta Crystallogr., Sect. A*, 1995, **51**, 33.
46 SAINT V6.2, Bruker Analytical X-Ray Systems, Madison, WI, 2001.
47 SHELXTL V6.10, Bruker Analytical X-Ray Systems, Madison, WI, 2000.